PCCP

Accepted Manuscript

ROYAL SOCIETY OF CHEMISTRY

www.rsc.org/pccp

Cite this: DOI: 10.1039/c0xx00000x

www.rsc.org/xxxxxx

ARTICLE TYPE

(Ti/Zr, N) codoped hematite towards the enhanced photoelectrochemical activity of water splitting

Haijun Pan,[a,b] Xiangying Meng,*[a,b] Dongyan Liu,[a,b] Song Li,[a] and Gaowu Qin*[a]

Received (in XXX, XXX) Xth XXXXXXXXX 20XX, Accepted Xth XXXXXXXXX 20XX

DOI: 10.1039/b000000x

In this theoretical study, first-principle calculations were carried out to explore the photocatalytic activity of cation (Ti or Zr) and anion (N) compensated codoping hematite based on density functional theory (DFT). For (Ti/Zr, N) codoped hematite, the band edges of conduction band and valence band move close to each other, leading to an obvious bandgap reduction. Compared with the pure hematite, the optical absorption coefficient of codoped hematite is significantly enhanced in the visible light region. The charge distribution at the conduction band minimum (CBM) and valence band maximum (VBM) is spatially separated after codoping, which is beneficial for extending the carrier lifetime. More interesting, the CBM becomes electronically delocalized in (Ti, N) doped hematite, which indicates a better carrier transport property in the bulk system. Due to these favourite features of (Ti/Zr, N) codoped hematite, an improved photocatalytic performance can be expected.

Introduction

Since the discovery of Fujishima–Honda effect,[1] much attention has been focused on looking for an appropriate semiconductor to efficiently convert solar energy to hydrogen energy by photoelectrochemical reactions. Because of its abundance, nontoxicity, and high chemical stability over a wide range of pH, hematite (α–Fe_2O_3) has been regarded as an available promising photocatalytic material in recent few years. Especially, the desired band gap (~2.1 eV) makes hematite utilize roughly 40% of the solar radiation.[2–4] If all photons with energy larger than 2.1eV are captured with a 100% quantum efficiency, the ideal energy conversion efficiency of hematite can reach 12.9% in the water splitting reaction.[5] However, the utilization of Fe_2O_3 is significantly hindered by its intrinsic shortages: First, pure hematite has a poor conductivity (<1 $cm^2 V^{-1} s^{-1}$), and a high electron–hole pair recombination rate (~10 ps), which lead to a short diffusion length about 2–4 nm;[6–8] Second, the electron transition is viewed as an indirect transition (*d–d* type), which is hard to be excited by photons in the visible region;[9–11] Last, the oxygen evolution reaction rate is low on the surface of Fe_2O_3.[12] Thus, it is necessary to weaken these disadvantages of Fe_2O_3 to meet the requirements of an ideal photocatalyst.

Experimentally, many techniques have been applied to improve the capacity of Fe_2O_3 in converting sunlight into hydrogen energy in past few years. Among them, doping heterogenous atoms into Fe_2O_3 has been commonly used to modify its photoactivity .[13-23] The functions of doping method are diverse, which are related to the increased electrical conductivity, charge carrier concentration, effective surface area, or modified surface properties. As for the weak light absorption in visible region, it is necessary to adjust the bandgap of hematite to ~1.7 eV.[24] So far, the limited reports regarding this subject refer to doping with Rh,[25] changing the shape– and size– of Fe_2O_3 nanocrystal,[26] as well as using the localized surface plasmon resonance.[27] Another frequently used method would be forming heterojunction with other semiconductor, which could be helpful to the photo-absorption enhancement, and separation of photo-excited electron-hole pairs.[28-30] In addition, lots of surface treatment strategies such as CoF_3, Al_2O_3, and Ga_2O_3 have been reported to elevate decomposition rate of water molecular on the surface.[31-33]

Given the complexity of experimental process, it is hard to figure out the origin of the enhanced photocatalytic activity. First-principles simulation has long been considered to be an effective method to explore the mechanism of experimental phenomena. Theoretically, investigating the doping effect has been an area in adjusting the electronic structure and optical properties of hematite. Huda et al. studied the electronic structure of 3d transition metal incorporated Fe_2O_3 with LSDA+U method.[34] They suggest that the incorporation of Ti would lead to the greatest increase in electrical conductivity among all the considered 3d transition metal atoms. Through GGA+U simulation, our group predicted that dopant Ru was a potential candidate in improving the photoactivity of Fe_2O_3 due to the enhanced conductivity.[35] Liao et al. studied electron mobility in doped hematite using electrostatically embedded clusters and the small polaron model.[36] They found that the Si (Ge) dopant did not trap electrons because of the difficulty for electron carrier to occupy the Si (Ge)–O anti-bonding orbital. The results of Ti/Si doped Fe_2O_3 obtained by Hybrid-DFT were reported to be quantitatively consistent with experimental data.[14] Due to the difficulty in monitoring the chemical reaction at the electrode-water interface, theoretical simulation has long been viewed as a

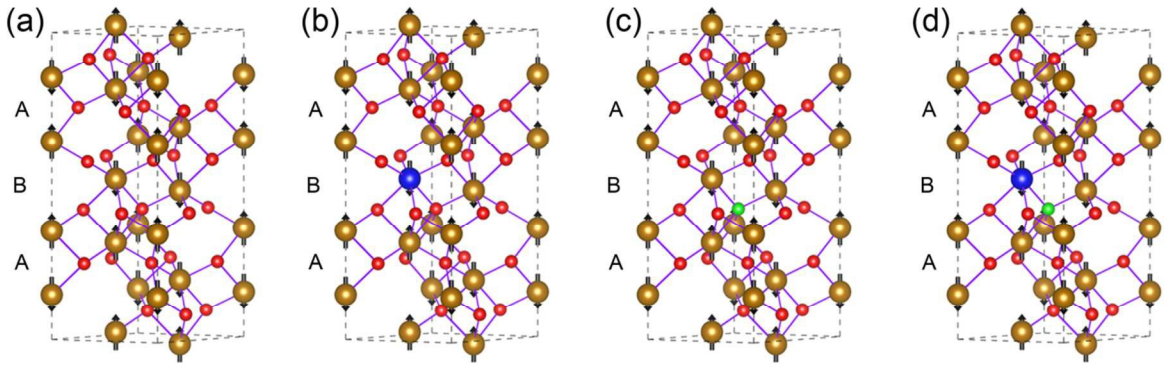

Fig.1 (a) Hexagonal close–packed crystal structure of pure hematite. Golden yellow and red spheres represent Fe and O atoms, respectively. The direction of magnetic moment at each iron atom is represented by the arrow. (b) The metal atom mono–doped hematite. The metal atom is incorporated into the position of a spin-down Fe atom, which is represented with blue spheres. (c) N mono–doped hematite. The O atom is replaced by N atom, which is labelled by green. (d) The cation and anion codoped hematite.

powerful tool to solve this challenge. Previously, a series of theoretical works showed that the dissociative adsorption of water molecules was energetically more favourable than the direct adsorption on Fe_2O_3 (0001) surface.[37-41] Using GGA+U method, our group investigated the reactive behaviour of single water molecule on Fe_2O_3 (0001) face, and showed the low energy barrier in the process of water dissociation.[42] Recently, the valuable work done by English et al. brought us new perspectives and knowledge.[43] They pointed out the dynamical properties of physically adsorbed water molecules, OH^- and H_3O^+ ions at complicated hematite/water interface with Born–Oppenheimer molecular dynamics (BOMD). These results on hematite/water interface would be a prerequisite for enhancing the chemical activity of Fe_2O_3 surface in the future.

As many researches do, this work also treats the improvement of bulk Fe_2O_3 properties as the primary objective. Unlike the mono-doping method, which may introduce impurity states in the bandgap, and cause a high recombination rate of photo-excited electron-hole pairs, doping semiconductor with anionic and cationic atoms simultaneously is an executable way not only to selectively tune the band edges, and drastically narrow the band gap, but also effectively avoid the impurity levels in the bandgap.[44, 45] Thus, we propose a compensated codoping approach to tune the electronic structure of hematite using the density functional theory (DFT) calculations. Our results indicate that hematite incorporated with metal ion (Zr or Ti) is an n–type semiconductor with a donor level in the band gap, while N doped hematite being p–type leads to an acceptor level. In (Ti/Zr, N) codoped hematite, the ascension of valence band maximum (VBM) and descension of CBM are the microscopic origins for the bandgap narrowing. Besides, the impurity levels, which may act as recombination centers, could be successfully eliminated in these codoped systems. Furthermore, the CBM is significantly affected in the case of (Ti, N) doped hematite, which indicates the improved electron mobility of hematite. Except for the favourable electronic properties, the formation energy indicates that the codoped hematite is thermodynamically stable, and can be prepared in the experiments. Our results show that the proposed codoped systems could efficiently improve the photoelectrochemical activity of hematite as a photocatalyst.

Computational detail and model

All calculations were performed in the framework of the spin–polarized density functional theory with Vienna *ab initio* simulation package (VASP) code.[46] The valence electron and ion core interactions were described by the projector augmented wave (PAW) potential.[47] For exchange correlation functional, the generalized gradient approximation of Perdew, Burk and Ernzerh (PBE) of was employed.[48] The cutoff energy of 550 eV was the maximum to expand the electronic wave function in plane wave. The Brillouin–zone integration was performed using Monkhorst–Pack grids of 11×11×10.[49] The lattice parameters and atomic positions of pure and doped hematite were fully relaxed using a conjugate gradient minimization algorithm until force convergence of 1 meV/Å and energy convergence of 10^{-5} eV are reached. The framework of GG+U invented by Dudarev et al. was selected in this simulation.[50] The value of U-J was set to 4.3eV, which was symmetrically picked out by Mosey et al.[51]

As shown in Figure 1a, hematite has a hexagonal close–packed crystal structure with a space group of R-32/C (NO.167), containing 12 Fe and 18 O atoms, which is always chosen to build doping models in previous research.[34, 35, 52] The experiments show that the hematite posses a stable antiferromagnetic (AFM) ground state below -10 ℃, in which the magnetic moment directions of iron are along the [0001].[53] There are two kinds of pairs of Fe atoms, which are denoted by a short Fe–Fe distance (type A) and by a larger distance (type B) along the hexagonal [0001] axis. Fe atoms of the type B have the same magnetic moment direction, whereas have the opposite direction in type A. To understand the properties of mono–doped hematite, substitutional doping is adopted, which is easier to form than interstitial doping (explained in Supplementary Information). In Figure 1b, a single metal atom (noted as M) is introduced by replacing a spin-down Fe atom to simulate the Ti/Zr doped hematite. As for N dopant, one of equivalent O atoms is substituted, which is displayed in Figure 1c. The compensated (Ti/Zr, N) codoped Fe_2O_3 is modelled by single substitution of a Fe atom by a metal atom, and one of its adjacent O atoms is

replaced by an N atom. Other possible codoping models are also carefully examined in Supplementary Information, which are not energetically favourable than above mentioned doping method. Besides, a 2×2×1 supercell consisting of 120 atoms is also constructed to simulate the pure and codoped hematite, which is also illustrated in Supplementary Information.

The prediction of optical properties helps us to understand optical photons interacting with the electrons in the pure and doped hematite. The absorption coefficient $\alpha(\omega)$ can be derived from the real and imaginary parts of the dielectric function as follow:[54]

$$\alpha(\omega) = \sqrt{2}\omega\left[\sqrt{\varepsilon_1^2(\omega) + \varepsilon_2^2(\omega)} - \varepsilon_1(\omega)\right]^{1/2}$$

Formation energy

We calculated the impurity formation energies for the doped hematite in order to know the growth mechanism and relative stability of new systems, according to the formula as follows:[55]

$$E(\text{M doped})_f = E(M\ doped) - E(pure) - \mu_{\text{M}} + \mu_{\text{Fe}}$$

$$E(\text{N doped})_f = E(N\ doped) - E(pure) - \mu_{\text{N}} + \mu_{\text{O}}$$

$$E(\text{codped})_f = E(codoped) - E(pure) - \mu_{\text{M}} + \mu_{\text{Fe}} - \mu_{\text{N}} + \mu_{\text{O}}$$

Where E(pure) is the total energy of hematite unit cell. E(M doped), E(N doped) and E(codoped) are the total energy of the systems containing M, N, and (M, N), respectively. μ_{M}, μ_{Fe}, μ_{N}, and μ_{O} represent the chemical potential of M, Fe, N, O, respectively. For Fe_2O_3, the restrictive condition between μ_{Fe} and μ_{O} is explained by the formula:

$$\mu_{Fe_2O_3} = 2\mu_{\text{Fe}} + 3\mu_{\text{O}}$$

As is well known, the impurity formation energy is closely related to the growth conditions, which could constantly vary from O–rich to Fe–rich conditions. In this study, we mainly focus on these two extreme conditions, namely, O–rich and Fe–rich conditions. Under Fe–rich growth condition, the chemical potential μ_{Fe} is calculated from the energy of one bulk Fe atom, and the corresponding μ_{O} can be obtained from above mentioned formula. Under O–rich condition, the chemical potential μ_{O} is determined by half of the energy of an O_2 molecule, and the μ_{Fe} can be calculated from the restrictive condition.

Table 1. Formation energies of doped hematite.

	Formation energy (eV)	
	Fe–rich	O–rich
Ti doped	-2.44	-3.86
Zr doped	-3.63	-5.05
N doped	4.56	5.51
(Ti, N) codoped	-0.11	-0.59
(Zr, N) codoped	-1.12	-1.59

The calculated formation energies for all doped hematite are listed in Table 1. It can be observed that in mono-doped hematite, the replacement of Fe atom with metal atom is easy to be realized, whereas N impurity is not readily incorporated into the crystal. The formation energy for metal atom substituting Fe atom in hematite is favourable under O-rich condition. In contrast, the formation energy for incorporating N atom is 4.56 eV under Fe-rich condition, which is less than 5.51 eV in the other condition. The compensated (M, N) codoped system is apt to be prepared under either Fe–rich or O–rich growth conditions, which is inferred by the negative formation energy. Furthermore, the results also show that the incorporation of metal atom must be prior to the appearance of N atoms in hematite. The subsequent N atoms are inclined to bond with metal atoms.

Electronic structure

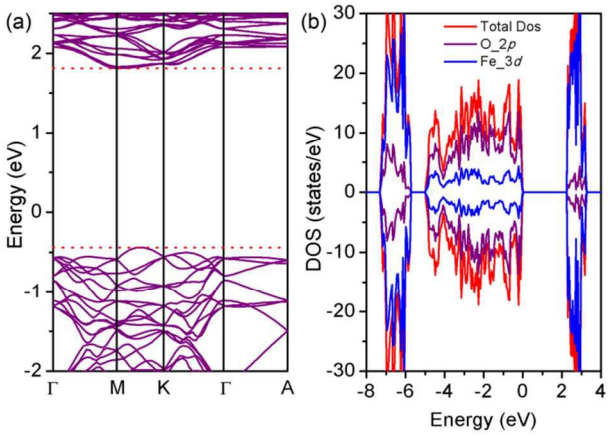

Fig.2 (a) The band structure and (b) density of electronic states (DOS) of pure hematite. The Fermi level is set to energy zero.

First, we need to check over the computational reliability of pristine hematite. From Figure 2, it can be found that the indirect bandgap of pure hematite is 2.25 eV. The localized Fe 3*d* states are the main component of nearly flat CBM, which indicates the heavy carrier effective masse in pure Fe_2O_3. It is one of the main reasons why high conversion efficiency has not been achieved with α–Fe_2O_3. On the other hand, the VBM is composed of Fe 3*d* and O 2*p* orbital, with O 2*p* electrons playing a dominant role. These results are consistent with the electronic properties calculated from 2×2×1 supercell, and previous computational observations.[34, 35, 52] As shown in Table 2, the lattice parameters obtained at 0K are a=b=5.07Å and c=13.88Å, which is in line with parameters measured at finite temperature. The calculated magnetic moment around iron atoms is 4.15μ_B. These comparisons ensure us to proceed with the theoretical design of the doped α–Fe_2O_3 catalyst.

Table 2.The structural parameter, bandgap, and magnetic momentum obtained by experiments and theoretical simulations

	a=b(Å)	c(Å)	E_g(eV)	μ_B
Expt.	5.029[56]	13.730[56]	2.1-2.3[2,16,57]	4.6-4.9[53,58,59]
Calc.	5.098[51]	13.915[51]	2.1[51]	4.2[51]
This work	5.07	13.88	2.25	4.15

When the O atom is substituted by the N atom, the acceptor states will be introduced because of one less valence electron than O. In band structure plot of N doped hematite shown in Figure 3a, a completely unoccupied impurity band is induced around the middle of band gap, and two half–filled energy levels emerge above the valence band edge. The Fermi level embeds in the

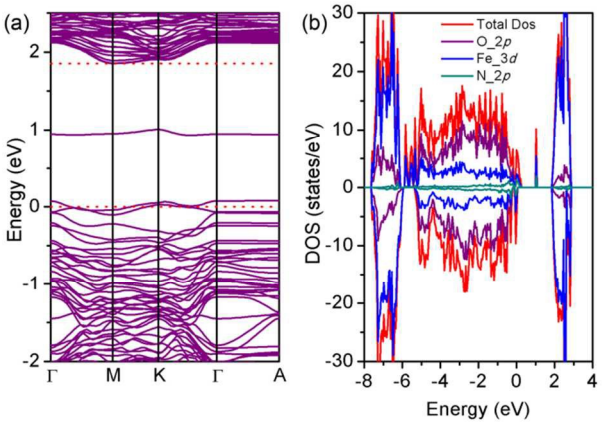

Fig.3 (a) The band structure and (b) density of electronic states (DOS) of N doped hematite. The Fermi level is set to energy zero.

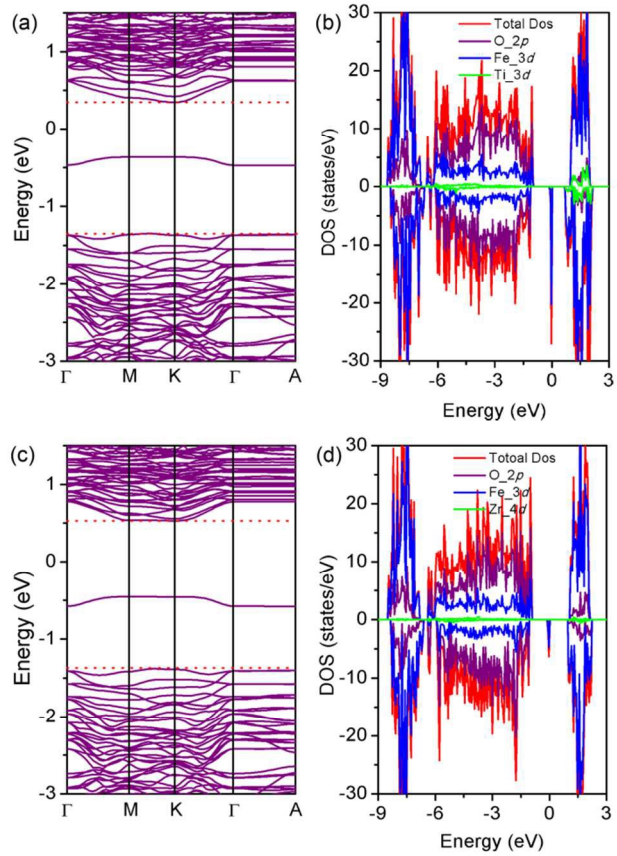

Fig.4 Band structure and DOS of Ti doped hematite (a and b) and Zr doped hematite (c and d). The Fermi level is set to energy zero.

VBM, and the N doped hematite should be viewed as a p–type semiconductor. Experimentally, the N doped hematite is well prepared, and identified as p-type through the typical cathodic photocurrent.[60] The calculated bandgap of the N doped system is 1.86 eV, which leads to an obvious band gap narrowing. To further explore the electronic structures of N doped hematite, the density of states (DOS) is calculated (as shown in Figure 3b). The DOS indicates that due to the higher N 2*p* orbital than the O 2*p* orbital, the introduction of N changes component of the VBM. In addition, the N 2*p* is mixed with the O 2*p* and Fe 3*d* orbital, which contribute to the shallow acceptor states in the middle of the bandgap and half–filled states above the VBM.

Next, we will explore the effect of doping with only Ti or Zr on the electronic structure of Fe_2O_3. As shown in Figure 4a, the replacement of Fe atom by 3d–transitional metal Ti leads to a donor level in the bandgap, which attribute to the extra electron provided by Ti. Experimentally, Deng et al. investigated the electronic structure of Ti-doped hematite, and suggested the increased donor density of hematite by Ti doping.[15] Besides, the nature of CBM has been significantly interrupted by incorporating Ti into hematite. The CBM of Ti doped hematite is inclined to shift toward the valence band and the band gap shrinks by about 0.28 eV. The CBM of Ti doped hematite becomes wavier than that of pure hematite, which may lead to a relative small effective electron mass. Thus, the excited electrons would be feasible to move to the surface and join the redox reaction, which is consist with the enhanced conductivity in experiment.[23] Figure 4b shows that the deep donor level appears in the band gap in the case of Ti doped hematite, and primarily possesses the Fe 3d electronic property. The mechanism of Ti doped hematite is first reported by Velev et al.[52] They point out that two *s* electrons and one *d* electron of Ti ($3d^2 4s^2$) are accommodated by the O 2*p* orbital, and the remaining 3*d* electron is higher in energy than the energy center of Fe 3*d* orbital, which flows to the nearby Fe atom, leaving Ti atom as Ti^{4+} cation. The Ti^{4+} ionic state for the Ti doping hematite is experimentally confirmed by the XPS.[21] Furthermore, the delocalized CBM is related to the presence of Ti 3d states. Due to the similar outer electronic structure with Ti, the replacement of Fe atom by 4d–transitional metal Zr also leads to a saturated impurity states in the forbidden gap, which is shown in Figure 4c and 4d. The concentration of free electrons is increased due to the introduction of donor level, which is experimentally confirmed by Mott–Schottky curve.[13] Moreover, the conduction band minimum of Zr doped hematite is inclined to shift toward the valence band, and the band gap shrinks by about 0.35 eV.

The above analysis indicates that mono–doping can effectively improve the photoactivity of hematite, but the introduced impurity level may act as recombination centres for the electron–hole pairs in bulk hematite. It is expected that the introduction of both p-type and n-type dopant elements could overcome this drawback of the individual element doping. Compared with mono-doped hematite, it can be seen from Figure 5 that the impurity levels do not emerge in the bandgap of (Ti/Zr, N) codoped hematite. Besides, the conduction band and valence band get close with each other, leading to a relative small bandgap. The bandgap reduce to 1.68 eV for (Ti, N) codoped hematite, and 1.70 eV for (Zr, N) codoped hematite, respectively. Accordingly, the cation-anion codoped hematite is much more effective for enhanced visible light absorption than undoped hematite, with higher quantum yield being achieved. As shown in Figure 5a, the more interesting characteristic is that the CBM of (Ti, N) codoped hematite becomes delocalized, which indicates a better carrier transport properties in the bulk system. The DOS

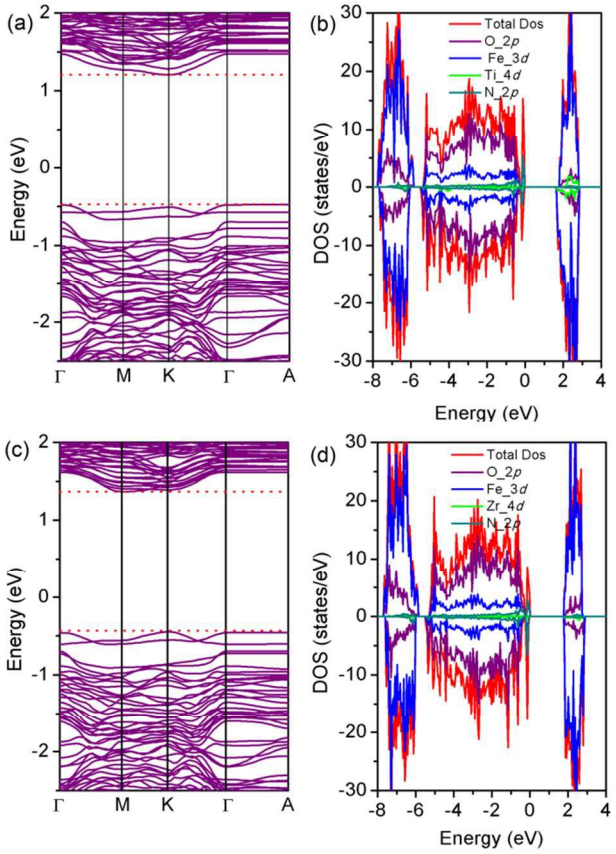

Fig.5 Band structure and DOS of (Ti, N) doped hematite (a and b) and (Zr, N) doped hematite (c and d). The Fermi level is set to energy zero.

patterns of compensated (Ti/Zr, N) codoped hematite are presented in Figure 5b and 5d, respectively. It can be observed that there is no obvious difference in the VBM in both the cases. Except for small amounts of O 2p and Fe 3d, the VBM is mainly attributed to the *d* electrons of doped metal atom and N 2*p* orbital, which is higher in energy than Fe 3*d* and O 2*p* orbital, respectively. However, the properties of the CBM of (Ti, N) codoped hematite and (Zr, N) codoped hematite differ significantly. In the case of (Ti, N) codoped hematite the CBM is composed of the Ti 3d and Fe 3d hybridized state, with the majority contribution from the Fe 3d state. While in the case of (Zr, N) codoped hematite, the CBM is only dominated by the Fe 3d state. Moreover, the codoping impact on the electronic structures of hematite is also examined using 2×2×1 supercell. The results shown in Fig.S6 demonstrate that the electronic properties of codoped hematite are invariable with the expended system size.

To check how dopants influence the band edge position, the variation of VBM and CBM of doped hematite is calculated according to the commonly used method,[61] which is shown in Figure. 6. The energy level of doped hematite is first corrected by aligning the average electrostatic potential of O atom located far from the doped atoms with that of the same atom in the pristine hematite. Then, the relative shift of VBM and CBM of doped system can be obtained. The result shows that incorporation of Ti and Zr can obviously alter the position of VBM and CBM at the

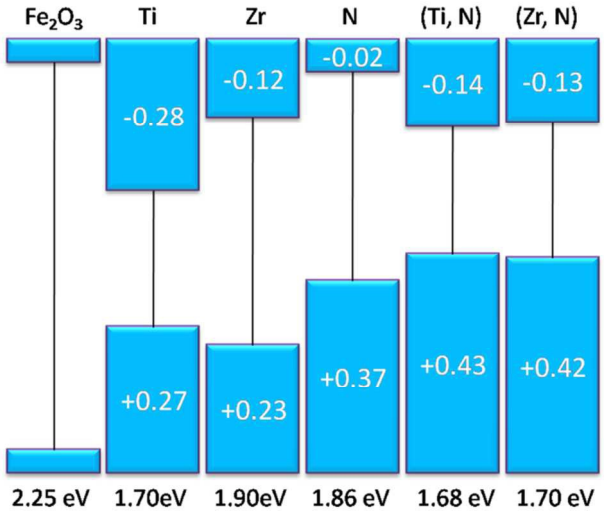

Fig.6 The computed band edge positions of doped hematite with respect to that of pristine hematite. Sign '–' and '+' indicates descend and ascend of CBM and VBM in doped hematite, respectively.

same time. With respect to the N doped hematite, the position of VBM is significantly elevated, leaving CBM nearly unchanged. In (Ti/Zr,N) codoped hematite, the VBM moves upward by ~0.4eV, which make most contribution to the bandgap reduction. The Bader charges around each atom are quantitatively calculated to further understand the charge transfer about the doped atom. In pure hematite, the calculated charges are -1.15e on the O atoms, and +1.73e on Fe centres, respectively. In the case of metal atom doped hematite, the Ti and Zr atom will donate 2.06e and 2.41e to form bonds with adjacent oxygen atoms, respectively. Compared with Fe atom (donate 1.73e), the doped Zr and Ti atom are easier to ionize, and form stronger coupling with surrounding O atoms. In N doped hematite, the charges around N atom are -1.05e from other atoms, which is smaller than O atom by 0.1e. In cation-anion codoped hematite, the charges on N atom increase to -1.27e in (Ti, N) doped hematite, and -1.32e in (Zr, N) doped hematite, respectively. The charges on metal atom are nearly the same as that in metal doped hematite.

In order to clearly show the change of the conduction band and valence band edges, we plot the band-decomposed charge density isosurface of the electronic states composing the band edge. As shown in Figure 7a and 7b, for pure hematite, partial charge density of CBM and VBM uniformly distributes around Fe atoms and O atoms, respectively. However, the spatial charge distribution is significantly changed by codoping. For (Ti/Zr, N) codoped hematite, the charge density distribution of CBM mainly spreads over Fe atoms far away from substitutional metal atom. The inflated charge density isosurface indicates the delocalized property of the electrons in conduction band. The spatially resolved electron density of VBM originates from the contribution of orbitals of N atom, and atoms surrounding N atom, respectively. These results are consistent with the above mentioned analysis of the energy band and DOS. In addition, the spatial separation of the charge density of VBM and CBM is helpful to avoid carrier recombination.

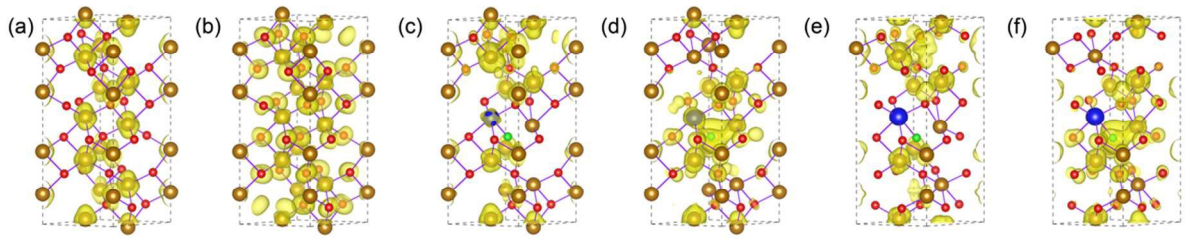

Fig.7 The band-decomposed charge density isosurface for the CBM and VBM of pure hematite (a and b), (Ti, N) codoped hematite (c and d), and (Zr, N) codoped hematite (e and f). Golden yellow, red, blue, and green atoms are Fe, O, metal atom, and N, respectively. The isosurface is 0.002 electrons per $Å^3$

Optical properties

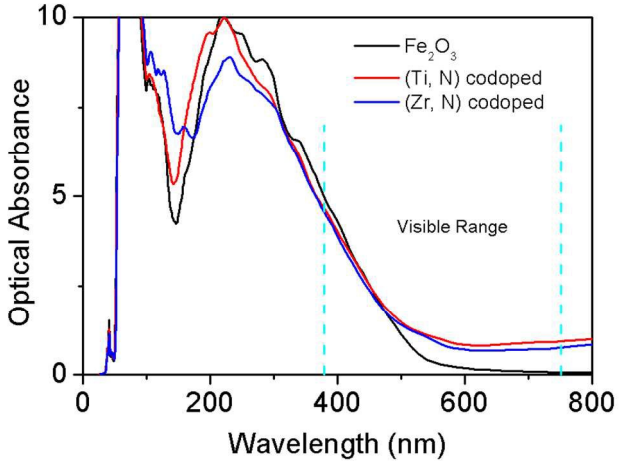

Fig.8 Optical absorption spectra of pure and codoped α–Fe2O3.

As a potential photocatalyst, it is important to investigate how the photons interact with the compensated (Ti/Zr, N) codoped hematite. Furthermore, the analysis of absorption property is an accurate complement of the electronic structure. The calculated absorption coefficients of pure and doped hematite are shown in Figure 8. It can be observed that pure Fe_2O_3 can strongly respond to the UV light and has weak absorption activity in the visible light region. The previous reports indicate that absorption of photons with wavelength around 550nm can be ascribed to the indirect transitions (Fe 3*d* ~ Fe 3*d*), which are not strongly absorptive in visible light range. The direct transitions (O 2*p* ~ Fe 3*d*) are active in the UV light region, corresponding to the absorption of photons with wavelength larger than 387nm.[9-11] With respect to codoped hematite, there are two aspects in common. As a result of the smaller bandgap (~1.70 eV), all photons with wavelength smaller than 740nm can be absorbed by codoped Fe_2O_3, exciting the electrons in valence band to conduction band. The (Ti, N) codoped hematite has an enhanced light absorption ability than the pure one from 450 nm, while the improved absorption coefficient begins with the wavelength of 510nm by (Zr, N) codoping. The essence of this enhancement originates from the shorter distance between Fe 3d states in VBM and CBM, which makes the indirect transition between Fe 3d easier. Besides, the photons with energy smaller than bandgap can also be captured by codoped hematite due to the intra-band transition in the valence band. However, there is distinct difference in ultraviolet region. The (Ti, N) codoping does not affect direct transition between O 2p and Fe 3d, while (Zr, N) doping make this transition weak.

Conclusion

In summary, electronic and absorption properties of compensated (Ti/Zr, N) codoping α–Fe_2O_3 have been investigated using first–principles calculations. These codoped systems show negative formation energies in different growth conditions, which make them more convenient to be prepared in experiment. The calculated electronic structure suggests that the codoping approch can effectively reduce the bandgap of hematite, leading to an excellent absorption property in the visible region. The charge distribution of CBM and VBM is spatially separated after codoping, which is beneficial for extending the carrier lifetime. More interesting, the CBM of (Ti, N) codoped hematite become delocalized, which indicates a better carrier transport properties in the bulk system. This simulation suggests that (Ti/Zr, N) codoped Fe_2O_3 may serve as promising photocatalytic materials in the future applications.

Acknowledgments

The authors gratefully acknowledge financial support by National Natural Science Foundation (No. 51001025 and No. 51002026), the Fundamental Research Funds for the Central Universities (No.130405003, No.11080001), Program for Changjiang Scholars and Innovative Research Team in University (No. IRT0713) and National High Technology Research and Development Program of China (Grant No. 2013AA031601).

Notes and references

[a] *Key Laboratory for Anisotropy and Texture of Materials (Ministry of Education), Northeastern University, Shenyang 110819, People's Republic of China*
[b] *College of Sciences, Northeastern University, Shenyang 110819, People's Republic of China*
**Corresponding authors. E-mail: x_y_meng@mail.neu.edu.cn* (XYM), *qingw@smm.neu.edu.cn* (GWQ)

1 A. Fujishima, K. Honda, Nature, 1972, 238, 37.
2 T. Bak, J. Nowotny, M. Rekas, C.C. Sorrell, Int. J. Hydrogen Energy 2002, 27, 991–1002.

3 P. Merchant, R. Collins, R. Kershaw, K. Dwight, A. Wold, J. Solid State Chem.1979, 27, 307–315.
4 A. Kay, I. Cesar, M. Grätzel, J Am Chem Soc, 2006, 128, 15714-15721.
5 A. B. Murphy, P. R. F. Barnes, L. K. Randeniya, I. C. Plumb, I. E. Grey, M. D. Horne, J. A. Glasscock, Int. J. Hydrogen Energy, 2006, 31, 1999.
6 R. Franking, L. S. Li, M. A. Lukowski, F. Meng, Y. Z.Tan, R. J. Hamers, S. Jin, Energy Environ. Sci. 2013, 6, 500–512.
7 N. J. Cherepy, D. B. Liston, J. A. Lovejoy, H. M. Deng, J. Z. Zhang, J. Phys. Chem. B, 1998, 102, 770–776.
8 J. H. Kennedy, K. W. Frese, Jr, J. Electrochem. Soc., 1978, 125(5), 709–714.
9 R. F.G.Gardner,F.Sweett, D.W. Tanner,J. Phys. Chem. Solids, 1963, 24, 1183–1186.
10 I.Balberg, H. L.Pinch, J. Magn. Magn. Mater., 1978, 7,12–15.
11 Z. Zhang, C. Boxall, G. H. Kelsall, Colloids Surf., A, 1993, 73, 145.
12 M. P. Dare-Edwards, J. B. Goodenough, A. Hamnett and P. R. Trevellick, Faraday Trans. 1, 1983, 79, 2027.
13 P. Kumar, P. Sharma, R. Shrivastav, S. Dass, V. R. Satsangi, Int. J. Hydrogen Energy, 2011, 36, 2777.
14 M. Rahman, N. Wadnerkar, N. J. English, J. M. D. MacElroy, Chem. Phys. Lett., 2014, 592, 242.
15 J. Deng, J. Zhong, A. Pu, D. Zhang, M. Li, X. Sun, S. T. Lee, J. Appl. Phys. 2012, 112, 084312.
16 J. A. Glasscock, P. R. F. Barnes, I. C. Plumb, N. Savvides, J. Phys. Chem. C, 2007, 111, 16477.
17 W. Cheng,J. He, Z. Sun, Y. Peng, T. Yao, Q. Liu, Y. Jiang, F. Hu,Z. Xie, B. He, S. Wei, J. Phys. Chem. C, 2012, 116, 24060–24067
18 X. Zhang, H. Li, S. Wang, Fu-Ren F. Fan, A. J. Bard, J. Phys. Chem. C, 2014, 118, 16842.
19 N. Mirbagheri, D. Wang, C. Peng, J. Wang, Q. Huang, C. Fan, Elena E. Ferapontova, ACS Catal., 2014, 4, 2006–2015.
20 M. Zhang, W. Luo, Z. Li, T. Yu, Z. Zou, Appl. Phys. Lett., 2010, 97, 042105.
21 C. Miao, T. Shi, G. Xu, S. Ji, C. Ye, ACS Appl. Mater. Interfaces, 2013, 5, 1310
22 A. Kleiman–Shwarsctein, Y. S. Hu, A. J. Forman, G. D. Stucky, E. W. McFarland, J. Phys. Chem. C, 2008, 112, 15900.
23 H. Muta, K. Kurosaki, M. Uno, S. Yamanaka, J. Alloys Compd., 2002, 335, 200-202.
24 G. W. Crabtree, M. S. Dresselhaus, M. V. Buchanan, Physics Today, 2004, 57(12), 39.
25 M. Seki, H. Yamahara, H. Tabata, Appl. Phys. Express, 2012, 5, 115801.
26 H. M. Fan, G. J. You, Y. Li, Z. Zheng, H. R. Tan, Z. X. Shen. S. H. Tang, Y. P. Feng, J. Phys. Chem. C, 2009,113, 9928.
27 P. Wang, B. Huang,Y. Dai, and Myung-Hwan Whangbo, Phys. Chem. Chem. Phys., 2012,14, 9813.
28 F. Achouri, S. Corbel, A. Aboulaich, L. Balan, A. Ghrabi, M. B. Said, R. Schneider, J. Phys. Chem. Solids, 2014, 75, 1081–1087.
29 M. Saleema, S. M. A. Durrani, N. Sahebc, M.F. Al-Kuhaili, I. A. Bakhtiari, Appl. Surf. Sci., 2014, 320, 653–657.
30 Y. Zhang, J. Gu, M. Murugananthan, Y. Zhang, J. Alloys Compd., 2015, 630, 110–116.
31 Y. S. Hu, A. Kleiman-Shwarsctein, G. D. Stucky and E. W. McFarland, Chem. Commun., 2009, 2652–2654.
32 F. Le Formal, N. Tétreault, M. Cornuz, T. Moehl, M. Grätzel, K. Sivula, Chem. Sci., 2011, 2, 737–743.
33 T. Hisatomi, F. Le Formal, M. Cornuz, J. Brillet, N. Tetreault, K. Sivula, M. Grätzel, Energy Environ. Sci., 2011, 4, 2512–2515.
34 M. N. Huda, A. Walsh, Y. F. Yan, S. H. Wei, M. M. Al-Jassim, J. Appl. Phys., 2010, 107(12), 123712.
35 H. J. Pan, X. Y. Meng, J. J. Cai, S. Li, G. W. Qin, RSC Advances, 2015, 5, 19353.
36 P. Liao, M. C. Toroker, E. A. Carter, Nano Lett., 2011, 11, 1775.
37 T. P. Trainor, A. M. Chaka, P. J. Eng, M. Newville, G. A. Waychunas, J. G. Catalano, and Jr. Brown, Surf. Sci. 2004, 573, 204.
38 S. Yamamoto, T. Kendelewicz, J. T. Newberg, G. Ketteler, D. E. Starr, E. R. Mysak, K. J. Andersson, H. Ogasawara, H. Bluhm, M. Salmeron, G. E. Brown, and A. Nilsson, J. Phys. Chem. C, 2010, 114, 2256.
39 C. M. Eggleston, A. G. Stack, K. M. Rosso, S. R. Higgins, A. M. Bice, S. W. Boese, R. D. Pribyl, and J. J. Nichols, Geochim. Cosmochim. Acta, 2003, 67, 985.
40 S. Yin, X. Ma, D.E. Ellis, Surface Science, 2007,601, 2426.
41 S. Yin, D.E. Ellis, Surface Science, 2008,602, 2047.
42 H. J. Pan, X. Y. Meng, G. W. Qin, Phys. Chem. Chem. Phys., 2014, 16, 25442
43 N. J. English, M. Rahman, N. Wadnerkar, J. M. D. MacElroy,Phys. Chem. Chem. Phys., 2014, 16, 14445.
44 Y. Gai, J. Li, S.-S. Li, J.-B.Xia, S.-H.Wei, Phys. Rev. Lett, 2009, 102, 036402.
45 W. -J. Yin, H. Tang, S. -H. Wei, M. M. Al-Jassim, J. Turner, Y. Yan, Phys. Rev. B, 2010, 82, 045106.
46 G. Kresse, J. Furthmüller, Phys. Rev. B, 1996, 54, 11169.
47 G. Kresse, D. Joubert, Phys. Rev. B, 1999, 59, 1758.
48 J. Perdew, K. Burke, M. Ernzerhof, Phys. Rev. Lett., 1996, 77, 3865.
49 H. J. Monkhorst, J. D. Pack, Phys. Rev. B 13 (1976) 5188.
50 S. L. Dudarev, G. A. Botton, S. Y. Savrasov, C. J. Humphreys, A. P. Sutton, Phys. Rev. B, 1998, 57, 1505.
51 N. J. Mosey, P. Liao, E. A. Carter, J. Chem. Phys, 2008, 129, 014103.
52 J. Velev, A. Bandyopadhyay, W. H. Butler, S. Sarker, Phys. Rev. B, 2005, 71, 205208.
53 F. J. Morin, Phys. Rev., 1950, 78, 819-820.
54 B. Modak, K. Srinivasu, S. K. Ghosh, Phys. Chem. Chem. Phys., 2014, 16, 17116.
55 J. Wang, H. Sun, J. Huang, Q. Li, J. Yang, J. Phys. Chem. C, 2014, 118, 7451–7457.
56 L. Pauling and S. B. Hendricks, J. Am. Chem. Soc., 1925, 47,781.
57 K. Sivula, F. Le Formal and M. Grätzel, ChemSusChem, 2011,4, 432.
58 L. W. Finger and R. M. Hazen, J. Appl. Phys., 1980, 51, 5362.
59 Y. Sato and S.-I. Akimoto, J. Appl. Phys., 1979, 50, 5285.
60 T. Morikawa, T. Arai, and T. Motohiro, Applied Physics Express 6,2013, 041201.
61 N. Umezawa, J Ye, Phys. Chem. Chem. Phys., 2012, 14, 5924.